JBIC (1999) 4:73–86 © SBIC 1999

ORIGINAL ARTICLE

**Paulo J. Martel · Cláudio M. Soares · António M. Baptista
Monika Fuxreiter · Gábor Náray-Szabó · Ricardo O. Louro
Maria A. Carrondo**

Comparative redox and pK_a calculations on cytochrome c_3 from several *Desulfovibrio* species using continuum electrostatic methods

Received: 31 August 1998 / Accepted: 20 November 1998

Abstract A comparative study of the pH-dependent redox mechanisms of several members of the cytochrome c_3 family has been carried out. In a previous work, the molecular determinants of this dependency (the so-called redox-Bohr effect) were investigated for one species using continuum electrostatic methods to find groups with a titrating range and strength of interaction compatible with a mediating role in the redox-Bohr effect. Here we clarify these aspects in the light of new and improved pK_a calculations, our findings supporting the hypothesis of propionate D from heme I being the main effector in the pH-dependent modulation of the cytochrome c_3 redox potentials in all the c_3 molecules studied here. However, the weaker (but significant) role of other titrating groups cannot be excluded, their importance and identity changing with the particular molecule under study. We also calculate the relative redox potentials of the four heme centers among the selected members of the c_3 family, using a continuum electrostatic method that takes into account both solvation and interaction effects. Comparison of the calculated values with available data for the microscopic redox potentials was undertaken, the quality of the agreement being dependent upon the choice of the dielectric constant for the protein interior. We find that high dielectric constants give best correlations, while low values result in better magnitudes for the calculated potentials. The possibility that the crystallographic calcium ion in c_3 from *Desulfovibrio gigas* may be present in the solution structure was tested, and found to be likely.

Key words Protein electrostatistics · Electron-proton coupling · Redox-Bohr effect · pK_a calculations · Cytochrome c_3

P. J. Martel (✉) · C. M. Soares · A. M. Baptista
R. O. Louro · M. A. Carrondo
Instituto de Tecnologia Química e Biológica, Universidade Nova de Lisboa, Apartado 127, P-2780 Oeiras, Portugal
e-mail: martel@itqb.unl.pt, Tel.: +351-1-4469613,
Fax: +351-1-4411277

M. Fuxreiter[1] · G. Náray-Szabó
Department of Theoretical Chemistry, Loránd Eötvös University, P. O. Box 32, H-1518 Budapest, Hungary

Present address:
[1] Department of Physiology and Biophysics, Mount Sinai School of Medicine, 1 Gustave L. Levy Place, New York, NY 10029-6574, USA

Introduction

Protein electron transfer is a molecular redox phenomenon central to respiratory, photosynthetic, and other energy transduction processes in biological systems [1]. Therefore, a great deal of effort has been put towards an understanding of its molecular basis, regulation, and structure-function relationships.

The bacterial tetrahemic cytochrome c_3 is a good system for studying protein electron transfer, given its small size (~100 aa), the availability of high-resolution X-ray [2–6] and NMR structures [7], and a wealth of available kinetic and thermodynamic data [8–13]. Cytochrome c_3 is found in the periplasm of all known species of sulfate-reducing bacteria, where it can act as proton-electron coupler between a hydrogenase and the electron-transport and ATP-synthesis transmembranar complexes [14].

The four heme centers of cytochrome c_3 are held together in close proximity, giving rise to both positive and negative cooperative effects between the redox potentials [10–13]. The redox potentials are pH dependent, and the nature of this dependency is also affected by the oxidation state of the molecule (this redox-pH coupling occurring in a physiologically meaningful context has been named redox-Bohr (R-B) effect [15, 16]). The electron-proton coupling implied by the redox-Bohr effect is particularly noteworthy, given the postulated role for cytochrome c_3 as a coupler to a periplasmic hydrogenase, with the simultaneous uptake of two electrons and two protons [10, 17].

Recent data on the pH dependence of this coupling supports the idea of concerted electron-proton transfer from the hydrogenase to cytochrome c_3 [14]. The thermodynamics of this system have previously been modeled by means of a binding model using four redox centers and one (or more) proton center [10, 18], with parameters describing the unknown cross interactions between the centers, the microscopic heme potentials, and proton binding constants. These parameters can be fitted to NMR and potentiometric data [10, 12, 13, 18]. Given the excellent quality of the fittings, the model microscopic potentials (hereafter simply referred as "model potentials") can be used as replacements for the unknown experimental microscopic potentials.

In a previous article [19], we used continuum electrostatic (CE) methods to investigate ionizable groups that could mediate the redox-Bohr effect in the cytochrome c_3 from *Desulfovibrio vulgaris* Hildenborough (DvHc3). Calculation of pK_a values, redox-dependent pK_a shifts, and charge-charge interactions between these groups and the heme centers allowed us to select some groups, based on titration range, magnitude of shift, and ranking of the interactions.

In this work, we improve this analysis for DvHc3 and extend it to another three members of the cytochrome c_3 family, namely those from *D. vulgaris* Miyazaki (DvMc3), *D. gigas* (Dgc3), and *D. desulfuricans* ATCC 27774 (Ddc3). Several concerns regarding the accuracy of the pK_a calculations have been addressed here (discussed in the Materials and methods section), giving rise to a substantial improvement in the calculated values. These improvements result in significant changes of the pK_a values of several key residues, allowing us to clarify some unsolved points in our previous work [19].

We also use CE methods to calculate relative microscopic heme potentials (see Materials and methods), and the results can be compared with the fitted potentials obtained with the multi-center model described above. The influence of the protein dielectric constant used in the CE method on the quality of the agreement between the two sets of results was analyzed in terms of the regression parameters of the linear fitting.

A coordinated calcium ion was found in the X-ray structure of Dgc3 [5], and its presence under in vivo conditions can be tested by running potential calculations with and without the calcium present in the structure, and comparing the results with the available data.

Materials and methods

Cytochrome structures

The crystallographic coordinates of cytochrome c_3 structures from *D. vulgaris* Hildenborough [2], *D. vulgaris* Miyazaki [3], *D. gigas* [5], and *D. desulfuricans* ATCC 27774 [6] were used in this work. In the case of DvHc3 there are two molecules in the asymmetric unit, and only molecule labeled "A" was used. Crystallographic water molecules were excluded from the calculations. The calcium ion present in the Dgc3 structure was included (see Results and discussion). When alternative conformations for side chains or parts of the structure were present in the crystallographic coordinates, the conformers with higher occupancy were used.

Atomic parameters

Charges on the protein atoms and ionizable groups in different protonation states were taken (or adapted) from the GROMOS87 force field [20] considering explicit polar and aromatic hydrogens [21]. The atomic radii used in the MEAD calculations (see below) were also taken from the GROMOS library, using the Lennard-Jones equation with two equivalent atoms and considering the radius to be half the distance corresponding to the minimum potential energy.

The charges for the redox centers in the oxidized and reduced states were calculated using ab initio quantum chemical calculations. The models of the redox centers were derived from hemes I and II of DvHc3, and comprised the following regions: the heme, the axial histidine, and covalently bound cysteine side-chains replacing C_α (CA) by hydrogen. Hydrogen atoms were added to complete the models, using the SYBYL modeling software (SYBYL Molecular Modeling Software, version 6a, Tripos Associates, St. Louis, Mo.).

Wave functions were obtained with GAUSSIAN94 [22], using unrestricted Hartree-Fock calculations with the STO-3G basis set. The convergence criterion was set to 0.0001.

Atomic charges were calculated by Mulliken population analysis of the calculated wave functions. The use of Mulliken analysis and a smaller basis set provides good agreement with experiment in other systems [23]. From the result of these calculations, sets of design charges for both the oxidized and reduced states were derived by comparing the results for both hemes in both redox states. The charges, shown in Table 1, were then used in the CE calculations described in the following sections.

Placement of titrable protons

The importance of a proper positioning of titrable protons was recently demonstrated by Alexov and Gunner [24]. This is a particular aspect of the relaxation effects that must be considered for correct evaluation of electrostatic energies in molecular systems (a full treatment can be carried out using the linear reponse approximation of Warshel and coworkers: see [25] for a complete study). Compared to our previous calculations [19], we see important differences in the calculated pK_a values when proton placement is done in several phases. First, fixed hydrogen atoms, i.e. the ones that can have only one conformation, were added using GROMOS [20]. Next, these structures were used for adding hydrogen atoms with variable conformation, i.e. the hydrogen atoms belonging to the end groups of Ser, Thr, Lys, Tyr, and Nterm, using the program WHAT IF [26], which implements an empirical potential for hydrogen bonding and optimization methodologies for hydrogen bond networks [27]. Finally, the titrable hydrogens belonging to Asp, Glu, and the propionates were positioned using the same procedure. Four possible positions are considered for hydrogen placement in carboxylic acids. This positioning was subsequently checked by visual inspection and corrections made when found necessary.

Given the positioning of all titrable protons in the protein structures, it is possible to use an explicit description of the protonation/deprotonation equilibrium in pK_a calculations. In some cases this is highly desirable, e.g. when one of the oxygen atoms of a carboxylic group is a hydrogen bond acceptor for a group belonging to another residue – in this case the proton should be added to the free oxygen atom. However, there are cases where this approach presents no advantage, such as when the titrable groups are totally exposed to the solvent and their mode of interaction cannot be derived in an obvious manner from examination

Table 1 Heme charges

Atom name	Charge	
	Oxidized	Reduced
Heme core		
FE	1.200	1.200
NA	−0.390	−0.405
NB	−0.390	−0.390
NC	−0.380	−0.405
ND	−0.400	−0.400
CHA	−0.085	−0.085
HCHA	0.120	0.095
C1A	0.110	0.040
C2A	0.000	0.000
C3A	−0.015	−0.055
C4A	0.110	0.110
CMA	0.035	−0.010
CAA	0.020	−0.005
CHB	−0.080	−0.140
HCHB	0.080	0.045
C1B	0.100	0.100
C2B	0.000	−0.040
C3B	−0.040	−0.040
C4B	0.090	0.030
CMB	0.035	−0.010
CAB	−0.070	−0.070
CBB	0.035	0.015
CHC	−0.100	−0.100
HCHC	0.070	0.045
C1C	0.090	0.040
C2C	−0.010	−0.010
C3C	−0.020	−0.055
C4C	0.105	0.105
CMC	0.020	−0.010
CAC	−0.065	−0.065
CBC	0.035	0.010
CHD	−0.090	−0.145
HCHD	0.080	0.045
C1D	0.110	0.110
C2D	−0.010	−0.050
C3D	0.000	0.000
C4D	0.100	0.025
CMD	0.050	0.000
CAD	0.020	−0.005
Cysteine 1 (attached to ring B)		
CB	−0.070	−0.070
SG	0.130	0.110
Cysteine 2 (attached to ring C)		
CB	−0.070	−0.070
SG	0.140	0.110
Axial histidines		
CB	0.005	0.005
CG	0.110	0.110
ND1	−0.305	−0.305
HD1	0.260	0.260
CD2	0.000	0.000
HD2	0.100	0.100
CE1	0.195	0.195
HE1	0.140	0.140
NE2	−0.305	−0.305

of the structure. In this case, an average description of the protonation/deprotonation process may be more adequate. The choice between average or explicit protonation is based on visual inspection of the environment of titrable residues. This procedure is applied only to the Asp, Glu, Tyr, and propionate groups; all other groups were assigned an average protonation state. The charges and model compound pK_a values used in the calculations are listed in Table 2. Explicit protonation charges are shown only for the cases where they were used.

pK_a calculations

All pK_a calculations were done using MEAD [28, 29] for the calculation of pK^{int} and site-site interactions. The model compounds for the MEAD calculations are the *N*-formyl-*N*-methylamide derivatives of the amino acid residues, but for the propionates only the atoms listed in Table 2 are used. This is necessary, in order to allow a clear separation between the redox and titrable fragments of the heme center. The model compound pK_a values (pK^{mod}) were taken from published data [30], except for the propionate pK^{mod}, which was set to that of acetic acid [31].

The electrostatic potential calculations in MEAD were performed using an 80 Å cube with a 1.0 Å lattice spacing centered on the protein, followed by a 20 Å cube with a 0.25 Å spacing centered on the titrating site. The ionic strength in the calculations was 0.1 M, approaching the in vivo ionic strength. The solvent probe radius was set to 1.4 Å, and the ion exclusion layer thickness was 2.0 Å, which approximates the sizes of counter ionic species in physiological conditions [32]. The external dielectric constant was set to 80 and the internal dielectric constant to 15. As discussed elsewhere [19], the use of such a high internal dielectric constant has, despite being questionable in physical terms, improved results when modeling experimental pK_a values [33, 34], probably owing to the exposed nature of the titrable residues and the reorganization effects missing from the continuum electrostatic treatment. In fact, the use of a high dielectric constant may compensate for the incomplete treatment of the reorganization energy of the protein dipoles [35–37]. This problem pertains also to the calculation of redox potentials (see Results and discussion).

For each pH value, the equilibrium distribution of protonation states was generated with our own software, which implements a Monte Carlo sampling of the protonation states [38, 39]. The Metropolis criterion was used in the transition (flips) of individual sites and strongly interacting pairs (interaction higher than 2 pH units). The p$K^{1/2}$ values (pH values for the titration midpoint) were then calculated from the titration curves.

Relative potential calculations

The free energy ΔG^{prot}_{redox} for the heme reduction in the protein

$$\text{Heme (oxidized)} + e^- \rightarrow \text{Heme (reduced)} \quad (1)$$

can be written

$$\Delta G^{prot}_{redox} = \Delta G^{wat}_{redox} + \Delta G_{solv} + \Delta G_{inter} \quad (2)$$

where ΔG^{wat}_{redox} is the redox free energy for the reduction of a His-His heme in water (without propionates), ΔG_{solv} is the energy change upon transfer of the heme to the protein interior, ΔG_{inter} is the interaction energy with the formal (full) charges in the protein (including the propionates and the other heme centers); the conformational changes upon reduction have been neglected (assuming these changes are small; see [40]). It must be noted that the solvation energy ΔG_{solv} is defined here as including both the Born cavity energy of placing the heme into a solvated low-dielectric cavity (as calculated for instance in [41]) *and* the interaction energy of the heme with the charges of all polar atoms in the polypeptide chain and the remaining three hemes (with the titrable residues in their neutral state). Interactions with the charged protonable groups and heme centers are grouped together in the ΔG_{inter} (this term depends on the chosen redox and protonation states of the protein). The relative redox free energy between water and protein, $\Delta\Delta G_{redox}$, is given by

$$\Delta\Delta G_{redox} = \Delta G^{prot}_{redox} - \Delta G^{wat}_{redox} = \Delta G_{solv} + \Delta G_{inter} \quad (3)$$

Table 2 Partial charges for titrable residues

	Charge protonated	Charge deprotonated
Arginine: pK^{mod} = 12.0		
CB	0.000	0.000
CG	0.000	0.000
CD	0.090	0.000
NE	−0.110	−0.150
HE	0.240	0.150
CZ	0.340	0.200
NH1	−0.260	−0.400
HH11	0.240	0.150
HH12	0.240	0.150
NH2	−0.260	−0.400
HH21	0.240	0.150
HH22	0.240	0.150
Lysine: pK^{mod} = 10.4		
CB	0.000	0.000
CG	0.000	0.000
CD	0.000	0.000
CE	0.127	0.000
NZ	0.129	−0.840
HZ1	0.248	0.280
HZ2	0.248	0.280
HZ3	0.248	0.280
Nterm: pK^{mod} = 7.5		
H1	0.248	0.280
H2	0.248	0.280
H3	0.248	0.280
N	0.129	−0.840
CA	0.127	0.000
CB	0.000	0.000
Histidine: pK^{mod} = 6.3		
CB	0.000	0.000
CG	−0.050	0.130
ND1	0.380	−0.580
HD1	0.300	0.000
CD2	0.000	0.000
HD2	0.000	0.000
CE1	−0.240	0.260
HE1	0.000	0.000
NE2	0.310	0.000
HE2	0.300	0.190
Tyrosine: pK^{mod} = 9.6		
CB	0.000 (0.000)	0.000
CG	0.000 (0.000)	0.000
CD1	−0.100 (−0.100)	−0.100
HD1	0.100 (0.100)	0.100
CD2	−0.100 (−0.100)	−0.100
HD2	0.100 (0.100)	0.100
CE1	−0.100 (−0.100)	−0.100
HE1	0.100 (0.100)	0.100
CE2	−0.100 (−0.100)	−0.100
HE2	0.100 (0.100)	0.100
CZ	0.150 (0.150)	−0.200
OH	−0.150 (−0.548)	−0.800
HH	0.000 (0.398)	0.000
Glutamate: pK^{mod} = 4.4		
CB	0.000 (0.000)	0.000
CG	0.000 (0.000)	0.000
CD	0.530 (0.530)	0.270
OE1	−0.265 (−0.380)	−0.635
OE2	−0.265 (−0.548)	−0.635
HE2	0.000 (0.398)	0.000
Aspartate: pK^{mod} = 4.0		
CB	0.000 (0.000)	0.000
CG	0.530 (0.530)	0.270
OD1	−0.265 (−0.380)	−0.635
OD2	−0.265 (−0.548)	−0.635
HD2	0.000 (0.398)	0.000
C-terminal: pK^{mod} = 3.8		
CT	0.530	0.270
O1	−0.265	−0.635
O2	−0.265	−0.635
Propionate: pK^{mod} = 4.75		
CBA	0.000 (0.000)	0.000
CGA	0.530 (0.530)	0.270
O1A	−0.265 (−0.380)	−0.635
O2A	−0.265 (−0.548)	−0.635
HO2A	0.000 (0.398)	0.000

[a] Values in parentheses are partial charges for explicit protonation

The influence of the protein environment in the modulation of the heme redox potentials can be examined by looking only at the relative redox potentials $\Delta\Delta G_{redox}$, avoiding the calculation or estimation of the heme reduction potential in water. $\Delta\Delta G_{redox}$ is related to the reduction potentials in water and the protein through the following equation:

$$\Delta\Delta G_{redox} = -F\Delta E = -F(E^{prot} - E^{wat}) \quad (4)$$

The terms ΔG_{solv} and ΔG_{inter} are mainly electrostatic in nature, and can be computed using a continuum method, e.g. as described in [42]. The choice of the proper dielectric constant for the protein interior has been the subject of extensive debate. It has been pointed out [43] that a single-valued dielectric description of the protein interior may not be able to produce correct results, given the presence of dipolar reorganization effects. We have adopted a more pragmatic view, in a manner similar to that described in [33], the major goal being the ability to reproduce the available experimental data. However, the effect of changing the protein dielectric constant has been also investigated in this work (see Results and discussion).

The actual calculation of ΔG_{solv} and ΔG_{inter} can be achieved using the MEAD software (see previous section), if we rewrite reaction 1 as:

$$\text{Heme (oxidized)} \rightarrow \text{Heme (reduced)} + e^{+} \quad (5)$$

where e^{+} is a unit positive charge. In this way, the redox process becomes formally equivalent to an acid-base process, and the heme groups can be treated as titrable cationic residues, with "ionized" and "neutral" forms corresponding respectively to the oxidized and reduced states. It can be easily seen that the ΔG_{solv} term is related to the heme "pK^{int}" through the following equation:

$$\Delta G_{solv} = 2.3RT\,pK^{int} \quad (6)$$

if we set the heme pK^{mod} as zero (this is the same as taking $E^{wat} = 0$ in Eq. 4, that is, taking the heme free energy of reduction in water as a reference value). The ΔG_{inter} terms are computed by summing up all the interactions between the heme group and the titrable residues (including the other heme groups in their reference, reduced state), as given in the MEAD output.

The parameters in the MEAD calculation were set as described in the section on pK_a calculations, and the charged forms for the oxidized and reduced heme were the previously described ones (see Table 1).

When comparing the calculated heme potentials against experimental values, it must be noted that the former are relative values and therefore only a linear correlation with unitary slope

should be observed, while the *Y*-intercept remains unknown but should be approximately constant across all the calculations (since it corresponds to the free energy of reduction of a solvated His-His heme without propionic groups).

Results and discussion

pK_a calculations

The MEAD calculated p$K^{1/2}$ values for the four cytochrome c_3 molecules are shown in Tables 3–6. The calculations were done for both the fully oxidized and fully reduced forms of the molecules, and the pK_a shifts upon full reduction are listed in the last column of the tables (see Materials and methods for details of the calculations). The pH midpoints of the redox-Bohr (R-B) transitions (see Introduction) have been derived from experimental redox and NMR data for the four c_3 species used here [10–13], and are listed in Table 7. The values for stage 0 and 4 correspond, respectively, to the fully oxidized and fully reduced forms of the molecules. Key groups in the R-B effect must titrate in the vicinity of the corresponding R-B range (Table 7) and are expected to display large reduction-linked pK_a shifts [19].

Table 3 pK_a calculations for DvHc3

Residue	p$K^{1/2}$		
	Oxidized	Reduced	Δ
NTALAavx-1[a]	6.9187	7.4063	0.4876
LYSavx-3	10.3658	10.6084	0.2426
ASPavx-7	2.1466	2.5558	0.4092
LYSavx-10	11.7578	11.9930	0.2352
GLUavx-12	4.1488	4.1267	−0.0221
LYSavx-15	10.6897	10.8224	0.1327
LYSavx-26	10.7712	10.9976	0.2264
LYSavx-29	11.3591	11.6286	0.2695
ASPall-32	2.9230	3.5359	0.6129
LYSavx-40	10.6655	10.8048	0.1393
GLUall-41	3.6021	3.9364	0.3343
ASPavx-42	1.8904	2.7648	0.8744
TYRall-43	12.6338	13.5456	0.9118
ARGavx-44	13.7205	14.1265	0.4060
LYSavx-45	12.4840	13.0540	0.5700
ASPall-53	1.9308	2.1632	0.2324
ASPall-56	3.1400	3.1674	0.0274
LYSavx-57	10.6815	10.9359	0.2544
LYSavx-58	10.0009	10.0090	0.0081
ASPall-59	2.5346	2.6862	0.1516
LYSavx-60	13.3706	13.7367	0.3661
LYSavx-63	11.6753	12.1230	0.4477
TYRall-65	16.0278	17.5768	1.5490
TYRavx-66	10.2085	11.8669	1.6584
HISBall-67[a]	7.6171	8.3706	0.7535
ASPavx-71	−0.8402	−0.2224	0.6178
LYSavx-72	9.7226	10.2603	0.5377
LYSavx-75	11.4661	11.7465	0.2804
LYSavx-77	12.2196	12.6775	0.4579
GLUavx-85	3.3162	3.6650	0.3488
ASPavx-90	2.1174	2.2077	0.0903
LYSavx-93	11.7789	11.9376	0.1587
LYSavx-94	10.5025	10.5939	0.0914
LYSavx-95	11.3317	11.5079	0.1762
ASPall-96	1.9411	2.2077	0.2666
LYSavx-101	11.1159	11.2819	0.1660
LYSavx-102	10.8157	10.9027	0.0870
LYSavx-104	12.1279	12.5497	0.4218
GLUavx-107	3.7312	3.8311	0.0999
CTGLUavx-107	2.4073	2.6467	0.2394
PropAI	3.4732	4.0313	0.5581
PropDI[a]	4.5426	6.2384	1.6958
PropAII	1.2371	2.2468	1.0097
PropDII[a]	4.2546	4.7789	0.5243
PropAIII[a]	3.3145	4.6175	1.3030
PropDIII[a]	4.5567	5.1578	0.6011
PropAIV	3.4672	4.0835	0.6163
PropDIV	1.4040	3.5926	2.1886

[a] Residues within ±1 pK_a units of the redox-Bohr range

Table 4 pK_a calculations for DvMc3

Residue	p$K^{1/2}$		
	Oxidized	Reduced	Δ
NTALAavx-1[a]	7.3125	7.4761	0.1636
LYSavx-3	10.5045	10.6587	0.1542
ASPall-7	3.1939	3.3344	0.1405
LYSavx-10	10.4931	10.8197	0.3266
ASPavx-12	3.1603	3.2266	0.0663
LYSavx-13	11.6351	12.0349	0.3998
LYSavx-15	10.7308	10.8130	0.0822
LYSavx-26	10.6563	10.8799	0.2236
LYSavx-29	11.2597	11.6928	0.4331
ASPall-32	2.2938	2.9493	0.6555
LYSavx-40	10.5161	10.6286	0.1125
GLUall-41	3.5012	3.8805	0.3793
TYRall-43	12.9580	13.8639	0.9059
LYSavx-45	12.2965	12.7226	0.4261
ASPavx-53	0.9507	1.2281	0.2774
ASPavx-56	3.1784	3.2470	0.0686
LYSavx-57	11.1207	11.3811	0.2604
LYSavx-58	10.7142	10.7196	0.0054
ASPavx-59	2.3330	2.5257	0.1927
LYSavx-60	13.0015	13.3461	0.3446
LYSavx-63	11.3322	11.7807	0.4485
TYRall-65	16.8203	18.5487	1.7284
TYRavx-66	10.1576	11.8425	1.6849
HISBall-67[a]	8.1893	8.9476	0.7583
ASPall-71	0.3376	0.9089	0.5713
LYSavx-72	10.4373	10.6197	0.1824
LYSavx-75	11.5891	11.9011	0.3120
LYSavx-77	12.1518	12.5536	0.4018
GLUavx-85	2.9129	3.2430	0.3301
ASPall-90	3.4267	3.4829	0.0562
LYSavx-93	13.6254	13.9940	0.3686
LYSavx-94	10.7164	10.8279	0.1115
LYSavx-95	10.3194	10.5046	0.1852
GLUavx-96	2.1607	2.4012	0.2405
LYSavx-101	10.6174	10.7018	0.0844
LYSavx-104	11.3109	11.7828	0.4719
CTSERavx-107	2.8146	3.0314	0.2168
PropAI	3.9836	4.6045	0.6209
PropDI[a]	4.6734	6.5105	1.8371
PropAII	1.4641	2.4577	0.9936
PropDII	3.0846	3.6676	0.5830
PropAIII	2.2006	4.1752	1.9746
PropDIII[a]	4.0632	4.7282	0.6650
PropAIV	3.9463	4.6604	0.7141
PropDIV	0.2076	1.9818	1.7742

[a] Residues within ±1 pK_a units of the redox-Bohr range

Table 5 pK_a calculations for Dgc3

Residue	p$K^{1/2}$		
	Oxidized	Reduced	Δ
NTVALavx-1[a]	7.9993	8.2996	0.3003
ASPavx-2	3.4336	3.5926	0.1590
ASPall-6	4.4903	4.7763	0.2860
LYSavx-9	10.8907	11.0478	0.1571
ASPall-11	1.5052	1.6582	0.1530
GLUavx-17	4.0409	4.1058	0.0649
LYSavx-18	10.5769	10.6805	0.1036
LYSavx-30	11.6959	11.8432	0.1473
ASPall-31	3.0372	3.3197	0.2825
LYSavx-33	12.7491	12.9309	0.1818
ASPall-35	2.4533	2.7766	0.3233
ASPall-36	2.2456	2.9854	0.7398
ASPavx-43	3.6574	3.7638	0.1064
LYSavx-44	10.4295	10.7566	0.3271
TYRall-46	11.0037	11.8234	0.8197
ASPavx-52	3.5640	3.6970	0.1330
ASPall-59	3.1314	3.2611	0.1297
LYSavx-60	11.2582	11.5107	0.2525
ASPall-62	3.3388	3.5449	0.2061
LYSavx-63	11.1580	11.1735	0.0155
TYRall-69	9.7672	11.5565	1.7893
LYSavx-70	12.0258	12.6026	0.5768
ASPall-74	1.5367	1.8960	0.3593
LYSavx-76	11.0029	11.0756	0.0727
LYSavx-80	12.0511	12.7793	0.7282
LYSavx-88	9.8992	10.3915	0.4923
ASPavx-89	3.5833	3.9062	0.3229
LYSavx-90	10.4634	11.8206	1.3572
ASPall-93	2.9807	3.0260	0.0453
ASPall-94	2.8429	2.9490	0.1061
LYSavx-95	10.5795	10.5904	0.0109
GLUavx-96	4.1820	4.2088	0.0268
LYSavx-98	11.6754	11.7741	0.0987
LYSavx-99	10.5044	10.5781	0.0737
LYSavx-100	11.7040	11.9999	0.2959
LYSavx-105	10.8473	11.0133	0.1660
CTPROavx-111	2.8936	3.1413	0.2477
PropAI	4.8195	5.1753	0.3558
PropDI[a]	4.5910	6.4058	1.8148
PropAII	2.3549	3.4640	1.1091
PropDII[a]	4.7051	5.2206	0.5155
PropAIII	3.4375	5.0832	1.6457
PropDIII[a]	4.7198	5.3385	0.6187
PropAIV	0.4619	1.6592	1.1973
PropDIV	−2.9020	−1.4319	1.4701

[a] Residues within ±1 pK_a units of the redox-Bohr range

Table 6 pK_a calculations for Ddc3

Residue	p$K^{1/2}$		
	Oxidized	Reduced	Δ
NTALAavx-1[a]	7.8296	8.0572	0.2276
LYSavx-7[a]	10.4138	10.5426	0.1288
GLUavx-10	3.2773	3.3841	0.1068
LYSavx-12	11.6521	11.8487	0.1966
LYSavx-16	10.8854	11.3941	0.5087
GLUall-26	3.0753	3.2872	0.2119
LYSavx-27	11.4999	11.7074	0.2075
GLUavx-29	3.9558	4.2299	0.2741
ASPavx-38	3.6490	3.7846	0.1356
LYSavx-40	10.9507	11.0624	0.1117
GLUavx-41	3.8115	4.0165	0.2050
TYRavx-43	11.5632	12.4083	0.8451
LYSavx-45	12.2207	12.6568	0.4361
ASPall-53	4.0620	4.2077	0.1457
ASPall-54	2.7014	2.7836	0.0822
LYSavx-58	12.2016	12.5718	0.3702
LYSavx-59[a]	10.5846	10.6820	0.0974
GLUavx-61[a]	4.9849	6.0399	1.0550
LYSavx-62	11.7155	11.8829	0.1674
TYRall-65[a]	8.8074	9.9423	1.1349
TYRavx-66	11.7557	12.1699	0.4142
LYSavx-71[a]	10.5884	10.9407	0.3523
GLUavx-73	3.8319	3.9076	0.0757
LYSavx-75	11.7758	12.0724	0.2966
HISBall-76[a]	6.5317	7.3743	0.8426
LYSavx-85	10.7172	11.0446	0.3274
GLUavx-89[a]	4.1373	4.3211	0.1838
LYSavx-90	12.2429	12.5052	0.2623
GLUall-92	4.1959	4.2373	0.0414
LYSavx-94[a]	10.1313	10.2648	0.1335
LYSavx-95[a]	9.0069	9.2534	0.2465
ASPavx-96	2.5925	2.9167	0.3242
LYSavx-102[a]	10.0306	10.0907	0.0601
LYSavx-104	12.0141	12.3128	0.2987
CTPROavx107	2.8769	3.0972	0.2203
PropAI[a]	4.2227	4.7555	0.5328
PropDI[a]	4.0065	5.9891	1.9826
PropAII[a]	4.6617	5.3337	0.6720
PropDII	2.0335	3.1742	1.1407
PropAIII[a]	4.4830	5.2703	0.7873
PropDIII	3.5703	4.2274	0.6571
PropAIV	3.0683	3.8968	0.8285
PropDIV[a]	6.4235	8.5176	2.0941

[a] Residues within ±1 pK_a units of the redox-Bohr range

Groups titrating within the R-B range (±1 pK_a unit) are indicated in Tables 3–6. It is clear that propionate DI (PropDI) is the only group that consistently displays a large shift and titrates in the expected region. The Nterm is in the R-B region in every case, but the redox-linked shifts are small. However, the pK_a calculations also suggest that PropDI cannot by itself describe the full range of the R-B effect – this is particularly noteworthy in the case of Ddc3. In the case of DvHc3, for example, the R-B midpoint occurs at 7.4 for the fully reduced form, although the calculated pK_a for PropDI is 6.2; His67 may be the cause for this displacement. Also, structural NMR studies in DvHc3 indicate strong interactions between PropDI and PropAI [7], pointing at the possibility of coupled proton uptake for these two residues. Although PropAI titrates below the R-B range of DvHc3, the above-mentioned coupling could bring its titration to a higher pH value (it is interesting to note that the observed R-B shift, 2.3, is equal to the sum of the calculated shifts of PropDI and PropAI).

If we compare DvHc3 with DvMc3, the 0.5 displacement in the R-B midpoint can be explained by the upward shift in the reduced and oxidized pK_a values of His67. In Dgc3, PropDI is again the residue with the major shift, but its range stays the same as in DvHc3 and DvMc3, while the R-B has a significant upward shift. Since the free His residue is absent from the Dgc3 structure, other groups must be the cause for this upward shift; the Nterm is a possible candidate, since its

Table 7 Redox-Bohr midpoints for the protonable group in the model of Turner et al. [10]

	Oxidation stage				
	0	1	2	3	4
DvHc3[a]	5.3	5.6	6.4	7.1	7.4
DvMc3[b]	5.9	6.2	6.9	7.4	7.8
Dgc3[c]	6.2	6.5	7.2	7.7	8.6
Ddc3(1)[d]	5.3	6.3	7.1	8.4	9.6
Ddc3(2)[d]	–	–	5.6	6.7	7.0

[a] Data from [10]
[b] Data from [18]
[c] Data from [12]
[d] Data from [13]

titration is shifted upwards, but again the possibility of coupled protonation between strongly interacting propionates cannot be excluded.

Further analysis of the MEAD calculation results shows that in DvHc3, DvMc3, and, to a less extent, in Ddc3, PropDI displays abnormal titration curves, extended over a large pH range. This is due, in the case of DvHc3, to a strong coupling with PropAI and Asp12 (results not shown). An abnormal titration behavior is also seen for PropDIV of Ddc3: a titration curve with biphasic character with shoulders around pH = 3 and pH = 7 (data not shown) in the fully oxidized state. It is plausible that titration of His67 and the Nterm influence the R-B upper midpoint in the case of DvHc3. Similar remarks can be made for the other three c_3 species, but the residues involved are different in each case. In the case of Dgc3, the redox-linked pK_a shift of PropDI has the same magnitude of the R-B shift, but it is lower by two pK_a units, and to observe R-B titration one needs to consider the Nterm and perhaps one or more residues in the upper titration range (e.g. Tyr69). In the case of Ddc3, the R-B effect is observed to cover a broad range [13], and this is substantiated in the calculations by the presence of a large number of residues showing significant shifts. The free His76 appears as potentially important group in the upper R-B range, with its redox-linked shift of 0.8 units (6.5–7.4).

The structure of Ddc3 used in this work was solved at low pH conditions ($\sim$4) [6], where some groups, like PropDIV and Glu61, are likely to be protonated, as can been seen by visual inspection. Thus the structure may be more accurate for describing a low-pH state than for the higher-pH, non-protonated state. Since a rigid structure was used over the whole pH range of the pK_a calculations, considerable errors may be present in the estimation of some pK_a values, particularly so for groups like PropDIV which interact strongly with their neighbors and may therefore suffer significant conformational changes upon protonation. As we will see in the section concerning potential calculations, the low pH/fully oxidized state was selected because it should match better the conditions under which the Ddc3 structure was solved. For this c_3 molecule, it seems that the observed R-B effect arises from the influence of a series of groups with overlapping titrations covering a wide range (cf. Table 6).

Residue-heme interactions

The interaction energies between heme centers and titrable residues were calculated using MEAD, as previously discussed in the Materials and methods section. The calculated values, presented in Figs. 1–4, correspond to the interaction energy of the fully ionized form of the residue with each heme center (the negative interactions with anionic residues are shown as positive for greater clarity). As expected, the highest interactions are those of the propionates with their corresponding hemes. However, for each of the four c_3 species there is an array of other groups which show considerable strength of interaction with the heme centers. The tyrosine residues belong to this category, but they must be discarded because of their calculated titration range, well outside the observed R-B zone. We have focused our attention on the residues presumably involved in the R-B effect (indicated in Tables 3–6):

- DvHc3. The Nterm has already been pointed out as a potential player in the R-B effect [19], and is seen to have a strong interaction with heme I. PropDI is particularly interesting because it interacts strongly with heme II, besides its own heme. His67, another potentially important residue, shows a strong interaction with heme II, and small but significant interactions with the other three hemes, so its influence in the R-B effect must be considered. Several Lys residues show considerable interactions with various hemes, but they titrate outside the R-B range. Among these, Lys45 is particularly interesting, because its replacement by an uncharged residue has been shown to disable the R-B effect in DvHc3 [44]; however, this is mostly due to its strong interaction with PropDI [19], giving further evidence for the key role of this residue.
- DvMc3. The picture is similar to that of DvHc3, except for a weaker Nterm interaction with heme I. This similarity is to be expected, given the structural homology between the two molecules. PropDI shows again a strong interaction with heme II.
- Dgc3. Other than the propionates and the Tyr residues, the strongest interaction is that of Lys90 with heme III. However, this residue titrates outside the R-B range for Dgc3, and since its conformation is not well defined in the X-ray structure, the calculated interaction may be affected by significant error. The free His residue is not present in the Dgc3 sequence.
- Ddc3. PropDI shows, as in the other three cases, a strong interaction with heme II, besides the one with its own heme. The free histidine, His76, appears again as having significant interactions, particularly with hemes I and II. Two other residues interact strongly with heme I: Glu61 and PropDIV.

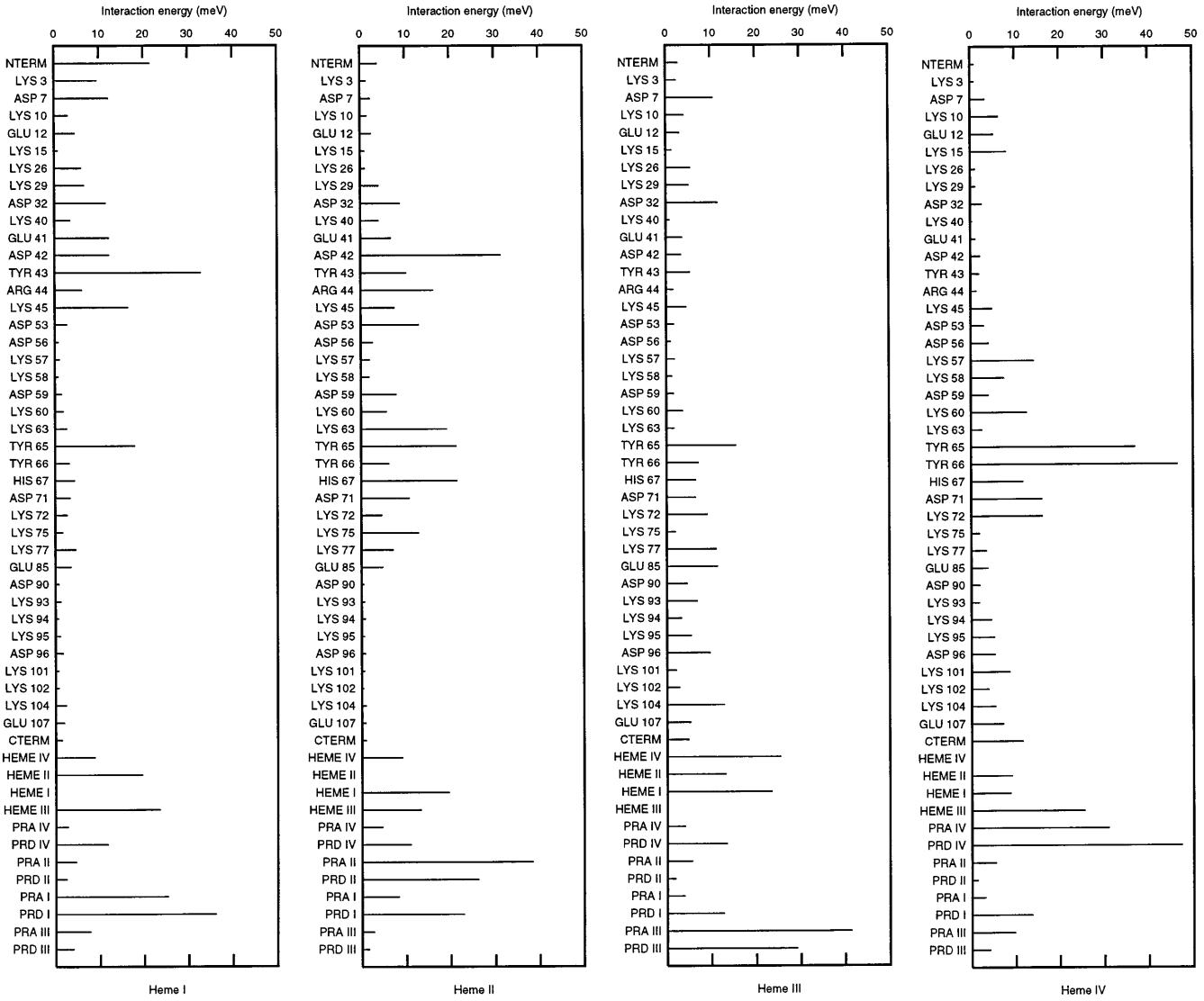

Fig. 1 Residue-heme interactions for DvHc3

Redox potential calculations

The calculation method for relative heme potentials described in the Materials and methods section was applied to the four cytochrome c_3 molecules. The calculated potentials can be compared with those obtained with the cooperative model of Turner et al. [10]. In this model, the pH-dependent behaviour is modeled through the inclusion of one or more acid-base groups, in addition to the four heme centers, by fitting the model parameters to experimental potentiometric and NMR data at various pH values [8, 10, 18, 45]. Microscopic redox potentials for the four heme centers can be obtained from this model for the protonated (low pH) and deprotonated (high pH) forms of the anionic group(s).

We have concentrated our attempts in the calculation of the first-stage reduction potentials from the fully oxidized forms of the c_3 species at low pH. This is because the X-ray structures used in this work have been determined at pH values below their R-B center titration point (see Table 7) and in their fully oxidized state [2, 3, 5, 6]. The ionization state of the titrable residues in the protein is set according to their calculated pK_a values and the range of the R-B effect in each case (Tables 3–6). For residues titrating in the R-B acidic range, the choice of protonation state is ambiguous. In the case of PropDI, the protonated state was chosen for consistency with both theoretical (see pK_a calculations above and [19]) and experimental evidence [46]. For other ambiguous residues, the protonation can be investigated by seeking a state which gives the best agreement with the available data on the microscopic potentials. This procedures gives additional information on which other residues may be involved in the R-B effect. The need to choose a set of protonation states disappears when calculations are made with a model that takes into account the simultaneous proton and electron uptake [47].

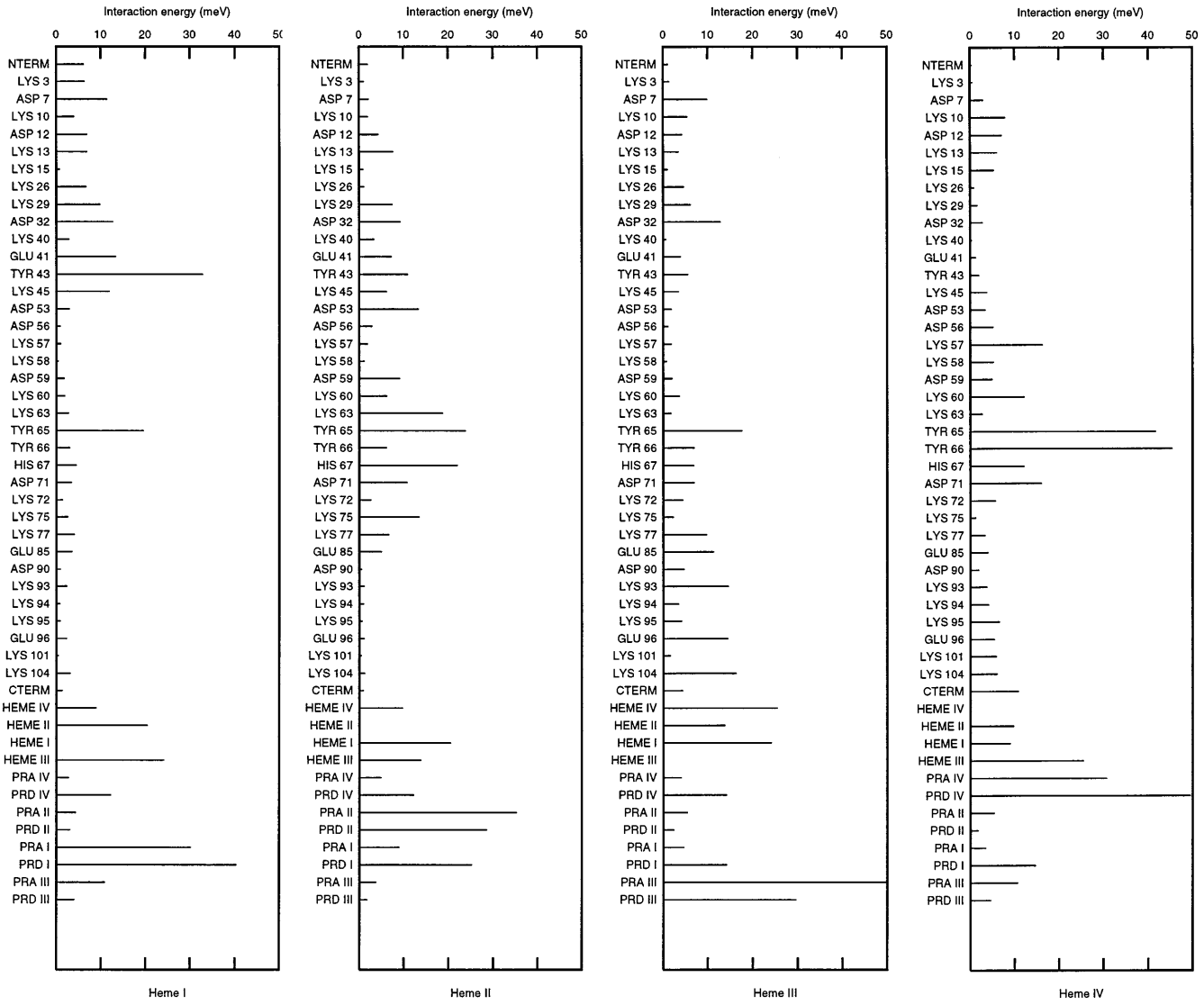

Fig. 2 Residue-heme interactions for DvMc3

The calculated heme potentials for the low-pH, fully oxidized forms of the four cytochromes were plotted against the microscopic heme potentials obtained with the thermodynamic multi-center model described above (Fig. 5). Table 8 lists the residues which were set at the fully protonated state for purposes of the calculation, and the slope, *Y*-intercept, and correlation values for each plot. The last row (labeled "All") corresponds to the total correlation for the 16 heme potentials taken together. Of the aforementioned ambiguous residues, the table also lists those cases where protonation leads to better correlation.

Observation of Fig. 5 shows a clear positive correlation between calculated and model potentials. However, the correct ordering of the heme potentials can only be reproduced in the case of Ddc3. The correlations (Table 8) are acceptable (except perhaps for Dgc3), but the slopes are much smaller than the unit value (as ideally expected). This scaling effect on the slopes is seen consistently and depends strongly on the value of the protein dielectric constant used in the CE calculations (see below). The same type of effect was observed in previous theoretical redox calculations using a free-energy perturbation method [19], although in this case the scaling displayed the opposite trend (slopes much greater than the unit value). According to our formalism (see Materials and methods), the *Y*-intercept of the

Table 8 Regression parameters for experimental versus calculated heme potentials

	Protonated residues	Correlation	Slope	*Y*-intercept
DvHc3	DI	0.74	0.61	183.7
DvMc3	DI, DIII	0.87	0.38	118.7
Dgc3	DI	0.68	0.15	52.61
Ddc3	AIII, AII, DI, DIV, E61	0.98	0.27	72.83
All	–	0.85	0.20	68.30

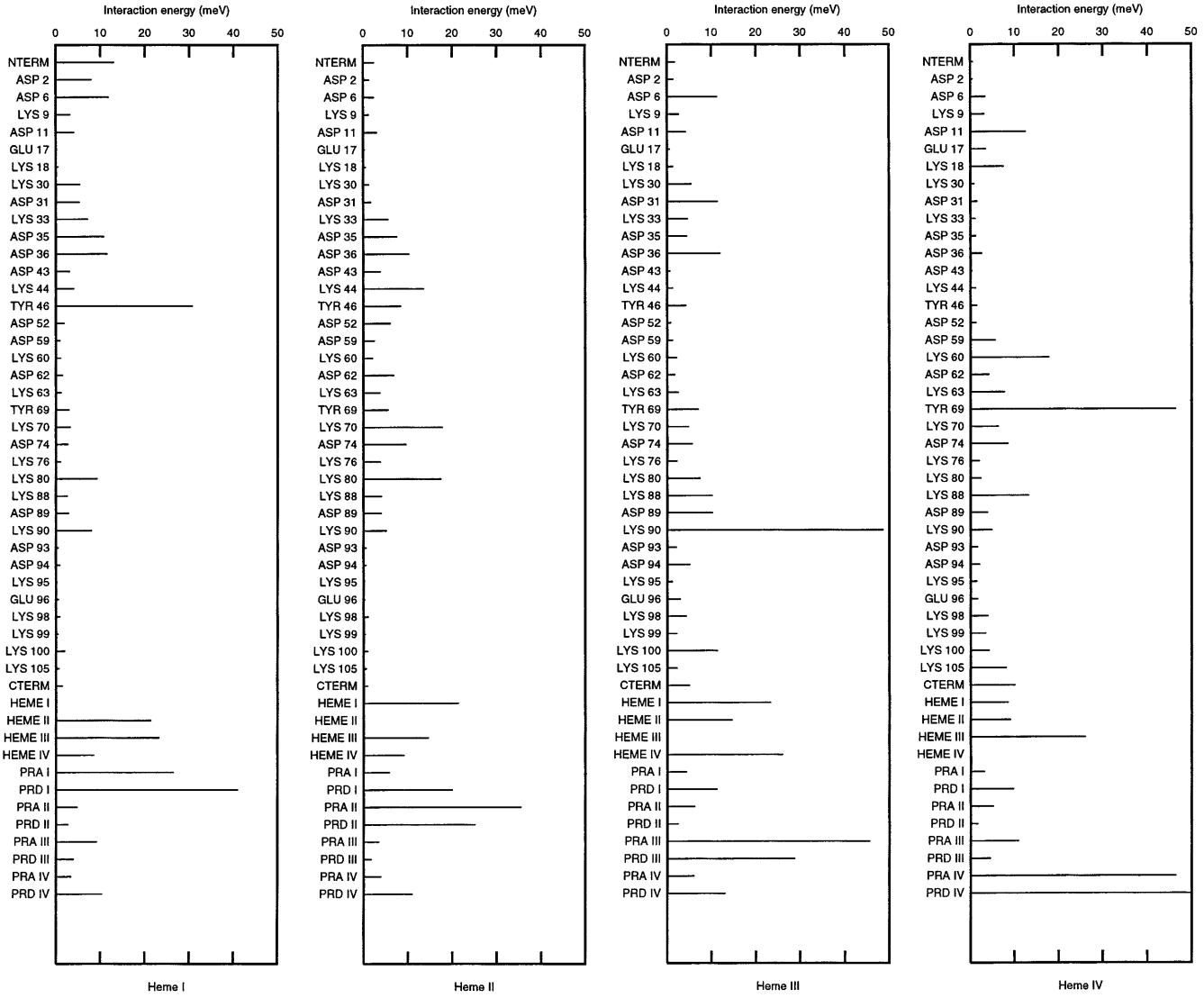

Fig. 3 Residue-heme interactions for Dgc3

plots should correspond to the (unknown) oxidation potential of our model compound. The value 183.7 mV obtained for DvHc3 seems reasonable when compared with the value for an His-His model heme (220 mV) [48] – the discrepancy could arise from the inclusion of an octapeptide in the model structure used in [48], an explicit effect of the propionate groups (absent from our model compound). However, the *Y*-intercept values for the other cases are much lower than could be expected. It must be noted that, because of the small number of points in each plot, the intercept values are highly sensitive to small deviations in the calculated values and therefore affected by significant error.

When the 16 hemes of the four cytochromes are plotted together, the picture is quite similar (Fig. 5). The correlation is reasonable, but the slope and *Y*-intercept are much smaller than would be desirable.

Effect of the protein dielectric constant

The use of a large dielectric constant for the protein has become customary in recent electrostatic calculations (e.g. [33, 49]). As pointed in [43], the use of a large protein dielectric constant for charge-charge interactions is a way of accounting for the missing conformational relaxation between charged states in an electrostatic calculation with a rigid protein model (a large effective dielectric constant between charged groups is observed when dielectric relaxation is treated explicitly with the linear response approximation of Warshel and coworkers – for a detailed study see [25]). Nevertheless, a small dielectric constant is still used for the computation of self-energies.

Previous work has reported the usage of a single protein dielectric constant of ~15 with improved results in the calculation of pK_a values and other molecular properties [33, 34].

In this section, we investigate the dependency of the calculations on the protein dielectric constant, based

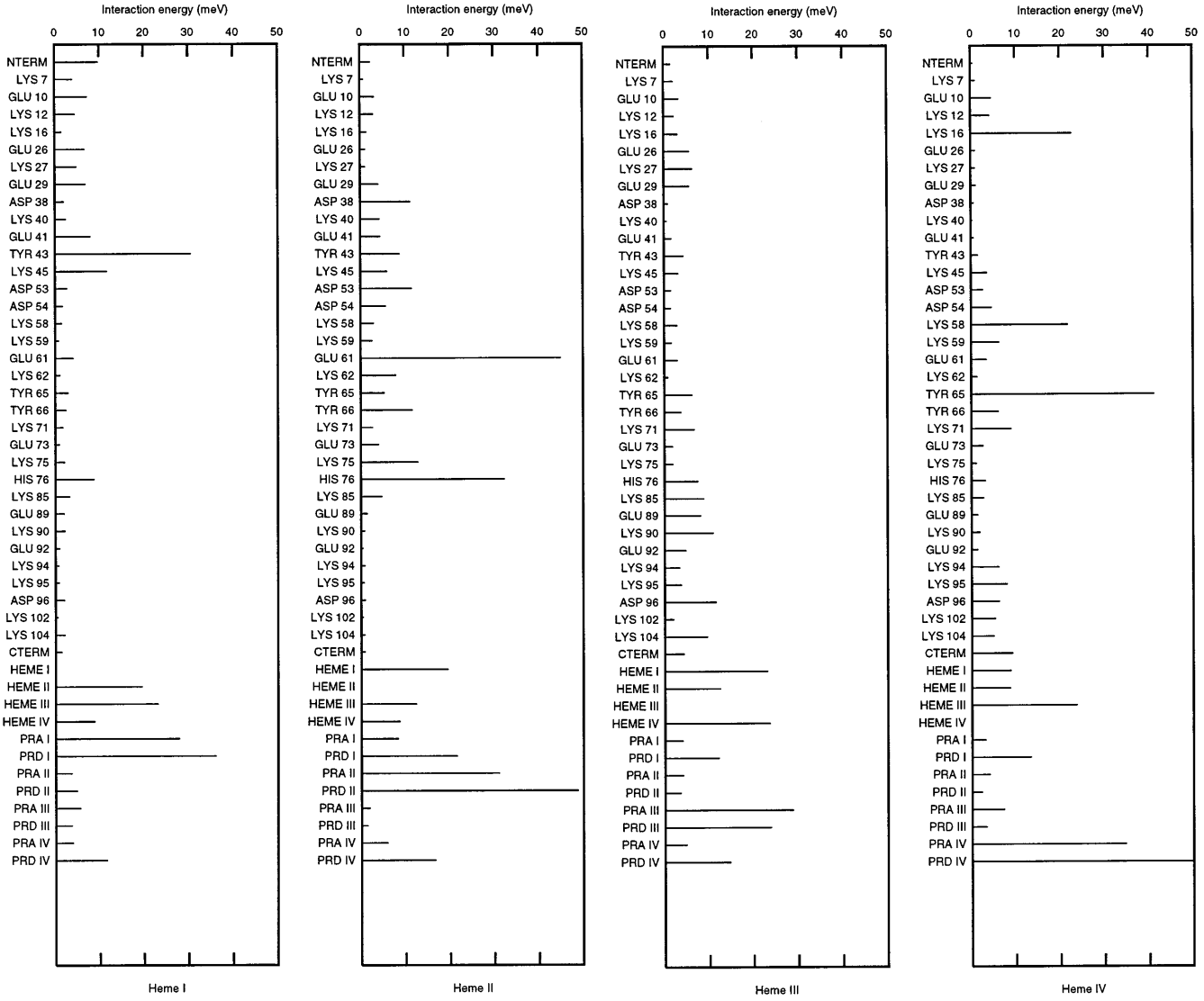

Fig. 4 Residue-heme interactions for Ddc3

solely on the potential plots described in the previous section. We considered again the low pH/fully oxidized situation, and performed calculations in a range of protein dielectric constants, searching for best correlation and slope values.

The effect of the protein dielectric is illustrated in Fig. 6 for the case of DvHc3. It is apparent that an increase in the dielectric constant results in improved correlation over a broad range of values. However, the expected unitary slope is attained for a dielectric constant ~ 5. Similar results are observed in the other three c_3 molecules (not shown). The *Y*-intercept approaches physically reasonable values (based on the redox potential of isolated hemes [48]), for values of the dielectric constant around 5. The rms deviation of the points from the fitted straight line is seen to decrease with the increase in dielectric constant. Lower dielectric constants for the protein result in correct magnitudes for the potentials, while larger values produce a better precision (less dispersion of the values). Overall it is difficult to make a definite conclusion, also because the potentials against which these calculations were compared are constrained by the nature of the fitted model used to derive them (description of the proton equilibria by means of one or a few titrable centers).

Presence of the calcium ion in the Dgc3 structure

The high-resolution structure of Dgc3 revealed the presence of a firmly bound Ca^{2+} ion in nearly perfect octahedral coordination, two of the six coordination atoms being the oxygens from the propionates A and D from heme IV [5]. Although the crystallographic data suggest that this ion is an integral part of the molecule [5], its presence in the solution (physiologically active) form of Dgc3 is an open question. A partial answer can be found by looking at the effect of the positive charge

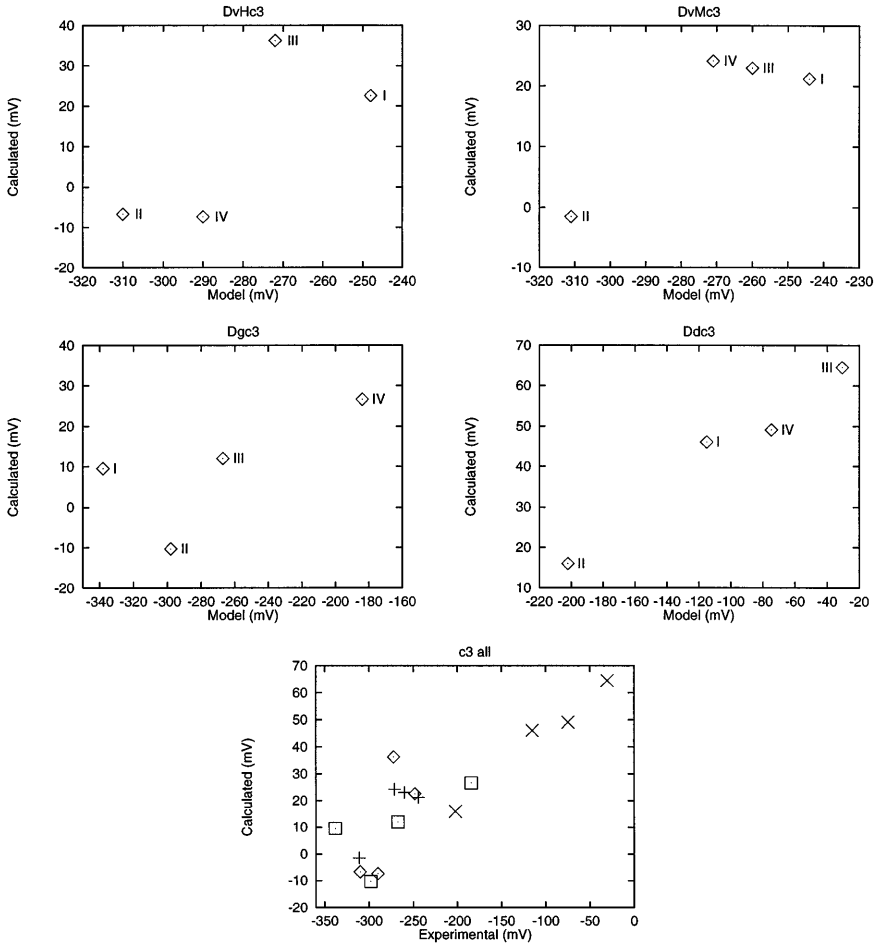

Fig. 5 Calculated heme potentials versus multi-center fitted models (data from [10], [18], [12], and [13]). All: DvHc3 (*diamonds*), DvMc3 (+), Dgc3 (*squares*), Ddc3 (×)

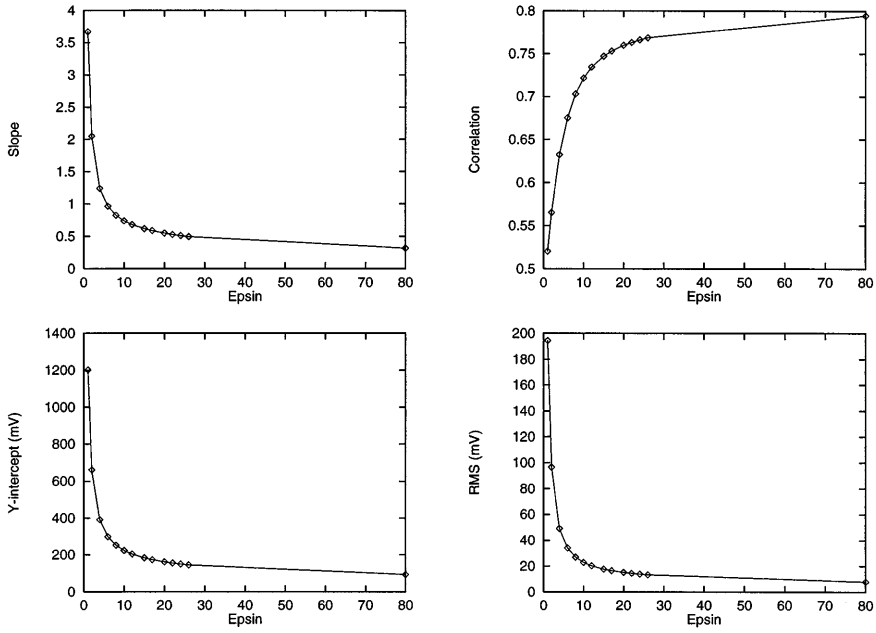

Fig. 6 Effect of the protein dielectric constant (Epsin) on the parameters for the fitting of calculated potentials (rms: root mean square deviation)

of the Ca^{2+} upon the heme redox potentials. If the Ca^{2+} ion is present, its positive charge should cause a significant upward shift in the heme potentials, particularly so in the heme nearest to it (heme IV). Calculations were run (using the previously described methods) on the Dgc3 structures with and without the calcium ion and the results compared with the fitted multi-center model potentials (derived from solution data; see potential calculations). In Fig. 7 it can be clearly seen that the presence of the Ca^{2+} ion results in signif-

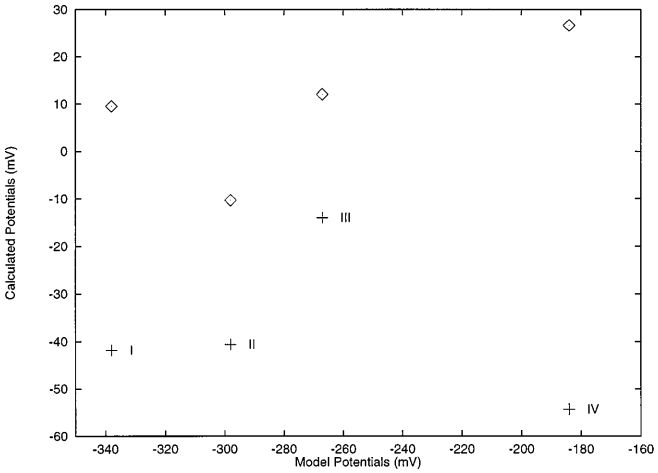

Fig. 7 Relative redox potentials in Dg with (*diamonds*) and without (*crosses*) the coordinated calcium ion. The correlation coefficients are 0.68 with calcium and −0.29 without calcium

icantly better agreement, with a correlation coefficient of 0.68 compared to −0.29 when the calculations are run without calcium. The differences are mostly due to the large downward potential shifts of hemes IV (80 mV) and I (50 mV) upon removal of the Ca^{2+} ion.

It must be noted that the removal of the Ca^{2+} ion for the purpose of the calculation should be followed by some process of conformational relaxation, in order to mimic the structural changes triggered by this process that must occur in the real structure. This is particularly relevant for propionates AIV and DIV since they complex the heme ion. Removal of the Ca^{2+} ion causes a jump of the pK_a values of these residues from 1.28 and −0.50 to respectively 6.80 and 6.32; in the real situation, this effect should probably be compensated by a structural relaxation of the propionates, allowing them to maintain low pK_a values. Instead of trying to simulate this relaxation process, we simply kept the pK_a values of these residues at their value in the calcium-containing structure.

Conclusions

The introduction of some improvements on the pK_a calculations for DvHc3 allowed us to reiterate the conclusion that propionate DI is the major effector in the redox-Bohr effect, at the same time eliminating other possibilities present in our previous work [19]. The free His and the amino terminal (Nterm) appear potentially important, their titration being more sensitive to the environmental changes through the various c_3 molecules studied here.

PropDIV shows a large shift upon reduction, but in a range below that of the R-B effect. However, the range of this shift could be extended through coupling with PropDI – this effect cannot be captured by the static CE model used in the calculations. The possibility of coupled behaviour of PropAI and PropDI in DvHc3 cannot be excluded, as indicated by structural NMR studies [7]. The calculations on DvMc3, Dgc3, and Ddc3 still point to PropDI as the most important effector in R-B; however, the role of other residues must be taken into account, particularly in the case of Ddc3, where the R-B effect occurs in a very broad range. The range and magnitude of the shift in PropDI is approximately constant in the four species, and so other residues must explain the wide variation in the observed R-B ranges. The free His and the Nterm display changes in their titration range which correlate well with the corresponding changes in R-B range for the different molecules. However, the free His is absent from the Dgc3 structure, and chemical blockage of the Nterm does not remove the R-B effect in DvHc3 [50].

The calculation of relative microscopic potentials for the hemes and their comparison with the values obtained with the thermodynamic model of Turner et al. [10] shows that quantitative results are not yet feasible, although the general trend of heme reduction can be reasonably predicted. The slope of the line of computed versus model potentials is well below the desirable unit value; this may be due to incorrect scaling of the electrostatic interactions, owing to an absence of flexibility effects or the use of an inappropriate value for the protein dielectric constant. This latter possibility was tested by changing the protein dielectric in a range of 1–80 and looking at the correlations, slopes, and *Y*-intercepts of the corresponding straight-line fits. The use of a higher dielectric constant clearly improves the correlation, but the "correct" unit slope is attained for low protein dielectric values (~5). The value of 15 that was used in this calculations seems to be a reasonable compromise between the two effects; however, a method that could account for conformational flexibility and thus avoid the use of an "artificial" dielectric constant would be desirable [51, 52].

The potential calculations for the Dgc3 structure with and without the calcium ion give support to the presence of this ion in the solution structure, even considering the likely errors in the calculated potentials, because the positive charge of the calcium and its proximity of hemes I and IV create a large upward shift in the reduction potential of these hemes that can be very easily seen in the calculations and should be well above the error range of the calculation. This result is in agreement with the strong association of the Ca^{2+} ion with Dgc3 reported in the crystallographic work [5].

Acknowledgements Prof. António V. Xavier is gratefully acknowledged for fruitful discussions and suggestions. This work is financially supported by PRAXIS XXI with grants BPD/4151/94 (C.M.S.), BPD/9967/96 (P.M.), BIC/1921/97 (A.M.B.), and by JNICT with PBIC/C/BIO/2037/95 and the Bilateral Luso-Hungarian Agreement (423/OMFB).

References

1. Bendall DS (ed) (1996) Protein electron transfer. Bios, Oxford
2. Matias PM, Frazão C, Morais J, Coll M, Carrondo M (1993) J Mol Biol 234:680–699
3. Higuchi Y, Kusonoki M, Matsuura Y, Yasuoka N, Kakudo M (1984) J Mol Biol 172:109–139
4. Morais J, Palma PN, Frazão C, Caldeira J, LeGall J, Moura I, Mouraq JJG, Carrondo MA (1995) Biochemistry 34:12830–12841
5. Matias PM, Morais J, Coelho R, Carrondo MA, Wilson K, Dauter Z, Sieker L (1996) Protein Sci 5:1342–1354
6. Simões P, Matias PM, Morais J, Wilson K, Dauter Z, Carrondo MA (1998) Inorg Chim Acta 273:213–224
7. Messias AC, Kastrau DHW, Costa HS, LeGall J, Turner DL, Santos H, Xavier AV (1998) J Mol Biol 281 (4):719–739
8. Santos H, Moura JJG, Moura I, LeGall J, Xavier AV (1984) Eur J Biochem 141:283–296
9. Catarino T, Coletta M, LeGall J, Xavier AV (1991) Eur J Biochem 202:1107–1113
10. Turner DL, Salgueiro CA, Catarino T, Legall J, Xavier AV (1996) Eur J Biochem 241:723–731
11. Salgueiro CA, Turner DL, Xavier AV (1997) Eur J Biochem 244:721–734
12. Louro RO, Catarino T, Turner DL, Piçarra-Pereira MA, Pacheco I, LeGall J, Xavier AV (1998) Biochemistry 37 (45):15808–15815
13. Louro RO, Catarino T, Turner DL, LeGall J, Xavier AV (to be published)
14. Louro RO, Catarino T, LeGall J, Xavier AV (1997) JBIC 2:488–491
15. Papa S, Guerrieri F, Izzo G (1979) FEBS Lett 105(2):213–216
16. Xavier AV (1985) In: Xavier AV (ed) Frontiers in bioinorganic chemistry. VCH, Weinheim
17. Louro RO, Catarino T, Salgueiro CA, LeGall J, Xavier AV (1996) JBIC 1:34–38
18. Salgueiro CA, Turner DL, LeGall J, Xavier AV (1997) JBIC 2:343–349
19. Soares CM, Martel PJ, Carrondo MA (1997) JBIC 2:714–727
20. van Gunsteren WF, Berendsen HJC (1987) Groningen molecular simulation (GROMOS) library manual. Biomos, Groningen
21. Smith LJ, Mark AE, Dobson CM, van Gunsteren WF (1995) Biochemistry 34:10918–10931
22. Frisch MJ, Trucks GW, Schlegel HB, Gill PMW, Johnson BG, et al (1995) Gaussian 94, revision B.2. Gaussian, Pittsburgh
23. Ramos MN, Gussoni M, Castiglioni C, Zerbi G (1988) Chem Phys Lett 151:397–402
24. Alexov EG, Gunner MR (1997) Biophys J 74:2075–2093
25. Sham YY, Muegge I, Warshel A (1998) Biophys J 74:1744–1753
26. Vriend G (1990) J Mol Graph 8:52–56
27. Hooft RWW, Sander C, Vriend G (1996) Proteins 26:363–376
28. Bashford D, Karplus M (1990) Biochemistry 29:10219–10225
29. You TJ, Bashford D (1995) Biophys J 69:1721–1733
30. Nozaki Y, Tanford C (1967) Methods Enzymol 11:715–734
31. Weasty RC (ed) (1984) Handbook of chemistry and physics. CRC Press, Boca Raton
32. Gilson MK, Honig B (1989) Proc Natl Acad Sci USA 86:1524–1528
33. Antosiewicz J, McCammon JA, Gilson MK (1994) J Mol Biol 238:415–436
34. Antosiewicz J (1995) Biophys J 69:1344–1354
35. Warshel A, Russell ST, Churg AK (1984) Proc Natl Acad Sci USA 81:4785–4789
36. Warshel A, Åqvist J (1991) Annu Rev Biophys Chem 20:267–298
37. Muegge I, Qi PX, Wand AJ, Chu ZT, Warshel A (1997) J Phys Chem 101:825–836
38. Antosiewicz J, Porschke D (1989) Biochemistry 28:10072–10078
39. Beroza P, Fredkin DR, Okamura MY, Feher G (1991) Proc Natl Acad Sci USA 88:5804–5808
40. Soares CM, Martel PJ, Mendes J, Carrondo MA (1998) Biophys J 74:1708–1721
41. Warshel A, Sussman F, King G (1986) Biochemistry 25:8368–8372
42. Gunner MR, Honig B (1991) Proc Natl Acad Sci USA 88:9151–9155
43. Warshel A, Papazyan A, Muegge I (1997) JBIC 2:143–152
44. Saraiva LM, Salgueiro CA, da Costa PN, Messias AC, LeGall J, van Dongen WMAM, Xavier AV (1998) Biochemistry 37:12160–12165
45. Salgueiro CA, Turner DL, Santos H, LeGall J, Xavier AV (1992) FEBS Lett 314:155–158
46. Park JS, Ohmura T, Kano K, Sagara T, Niki K, Kyoguku Y, Akutsu H (1996) Biochem Biophys Acta 1293:45–54
47. Baptista AM, Martel PJ, Soares CM (1998) (in press)
48. Harbury HA, Cronin JR, Fanger MW, Hettinger TP, Murphy AJ, Myer YP, Vinogradov SN (1965) Proc Natl Acad Sci USA 54:1658–1664
49. Martel PJ (1996) PhD thesis, New University of Lisbon
50. Saraiva LM, Salgueiro CA, LeGall J, van Dongen WMAM, Xavier AV (1996) JBIC 1:542–550
51. Baptista AM, Martel PJ, Petersen SB (1997) Proteins 27:523–544
52. Warshel A, Papazyan A (1998) Curr Opin Struct Biol 8:211–217